scientific reports

Check for updates

OPEN

Magnetic yolk-shell structured periodic mesoporous organosilica supported palladium as a powerful and highly recoverable nanocatalyst for the reduction of nitrobenzenes

Meysam Norouzi, Dawood Elhamifar✉ & Shiva Kargar

A novel palladium-loaded yolk-shell structured nanomaterial with magnetite core and phenylene-based periodic mesoporous organosilica (PMO) shell (Fe_3O_4@YS-Ph-PMO/Pd) nanocatalyst was synthesized for the reduction of nitrobenzenes. The Fe_3O_4@YS-Ph-PMO/Pd was prepared through cetyltrimethylammonium bromide (CTAB) directed condensation of 1,4-bis(triethoxysilyl) benzene (BTEB) around Fe_3O_4@silica nanoparticles followed by treatment with palladium acetate. This nanocatalyst was characterized by using Fourier transform infrared (FT-IR) spectroscopy, thermal gravimetric analysis (TGA), low-angle and wide-angle powder X-ray diffraction (PXRD), scanning electron microscopy (SEM), transmission electron microscopy (TEM) and vibrating sample magnetometer (VSM) analyses. These analyses showed a magnetic nanomaterial with high chemical and thermal stability for the designed composite. The Fe_3O_4@YS-Ph-PMO/Pd nanocomposite was employed as a powerful and highly recoverable catalyst in the green reduction of nitroarenes in H_2O at room temperature. A variety of nitroarene derivatives were applied as substrate in the presence of 0.9 mol% of Fe_3O_4@YS-Ph-PMO/Pd catalyst. All nitroarenes were selectively converted to their corresponding amines with high to excellent yields (92–96%) within short reaction times (10–18 min). This catalyst was recovered and reused at least 11 times without significant decrease in efficiency and stability.

Keywords Magnetic yolk–shell structured nanocomposite, Periodic mesoporous organosilica, Reduction of nitroarenes, Green conditions

In the recent years, the yolk-shell (YS) structured nanomaterials have demonstrated a new type of structures containing a void between core and shell. These materials have received increasing attention owing to tunable their physiochemical properties and also high capability in the adsorption and catalytic processes[1–9]. These nanomaterials have a lot of application in areas of data storage, catalysis and environmental remediation[5,6,10–12]. Due to the aforementioned notes and also widespread applications of YSs in green chemistry, various methods such as Kirkendall, etching, ship in bottle and Ostwald have been employed for the synthesis of these materials[13–16]. Among these, selective etching is very interested in between researchers[17,18]. YSs with magnetite core and PMO shell (Mag@YS-PMOs) have attracted much research attention because of their combined properties of YSs, magnetic materials and ordered mesoporous structures[12,19–22]. The Mag@YS-PMOs have the advantages of magnetic nanoparticles such as easy magnetic separation, high dispersion ability in aqueous media as well as high chemical reactivity and stability. In addition, these have also the advantages of PMOs such as highly-ordered mesostructure, excellent loading of uniformly distributed organic functions in their framework and high moisture stability[12,19,23]. These characteristics make Mag@YS-PMOs as promising applicant for supporting metals in different chemical processes[5,6,24,25].

Department of Chemistry, Yasouj University, Yasouj 75918-74831, Iran. ✉email: d.elhamifar@yu.ac.ir

On the other hand, aromatic amines are very important in herbicide, dye, agrochemical and pesticide industries[26–28]. In addition, they are substrates for different intermediates such as diazonium salts, isocyanate, azo and amide molecules[29,30]. Recently, sodium borohydride, $NaBH_4$, has been suggested as a new fuel source for supplying hydride ions to reduce nitroarene compounds to the corresponding amines under mild conditions. However, $NaBH_4$ exhibits limited capability in the absence of additives[31–35]. Therefore, this reagent is usually used in the presence of metallic catalysts. Another important and conventional method for preparing the aromatic amines is the reduction of corresponding nitroarenes via catalytic hydrogenation[36,37]. The most metallic complexes and metallic nanoparticles applied for catalytic reduction of nitroarenes are based on Rh, Ru, Pt, Pd, Au, Cu, Ir and Ni[38–40]. Some of recently developed catalytic systems in this matter are Fe_3O_4/Ni MNPs[41], Rh–Fe_3O_4 heterodimer[42], Cu/Fe_2O_4–G[43], graphene-Fe_3O_4[44], Au–GO[45], Fe_3O_4@GO[46], Ag@Ni[47] and $NiFe_2O_4$@Cu[48]. However, the homogeneous protocols for reduction of nitroarenes have different disadvantages such as separation of catalyst and product. Therefore, it is still necessary to design an effective catalytic system resolving these issues.

According to the advantages of Mag@YS-PMO-based nanocatalysts as well as the importance of reduction of nitroarenes in green chemistry, in continuation of our previous works[49–51], herein, a YS nanomaterial with magnetite core and PMO shell-supported palladium species (Fe_3O_4@YS-Ph-PMO/Pd) is synthesized through sol–gel mediated hydrolysis and co-condensation of 1,4-bis(triethoxysilyl)benzene (BTEB) around Fe_3O_4@SiO_2 cores using CTAB surfactant followed by treatment with palladium acetate (Fig. 1). Furthermore, the physiochemical properties of the synthesized Fe_3O_4@YS-Ph-PMO/Pd nanocatalyst were studied by using FT-IR, TGA, PXRD, SEM, TEM and VSM techniques. After characterization, the catalytic efficiency of this magnetic nanomaterial was investigated in the green reduction of nitroarenes under moderate conditions.

Experimental

General

All chemicals and reagents such as iron (II) chloride tetrahydrate, iron (III) chloride hexahydrate, ammonia, 1,4-bis(triethoxysilyl)benzene, $NaBH_4$, cetyltrimethylammonium bromide (CTAB) and all applied nitroarenes and alcohols were purchased from Fluka, Merck and Aldrich companies. Solvents were dried and purified following standard procedures. The characterization of the materials was conducted using instruments previously reported[52,53]. The purity determination of the products and reaction monitoring were carried out by using TLC on silica gel polygram SILG/UV 254 plates.

Preparation of Fe_3O_4@YS-Ph-PMO

For the preparation of Fe_3O_4@YS-Ph-PMO nanomaterial, firstly, Fe_3O_4 and silica coated magnetite nanoparticles (Fe_3O_4@SiO_2) were synthesized according to known procedures[23]. Then, 100 mg of Fe_3O_4@SiO_2 microspheres were added into a flask containing EtOH (60 mL) and H_2O (80 mL). This mixture was homogenized for 25 min under ultrasound irradiations. Next, CTAB (140 mg) and NH_3 (25%, 2 mL) were added while stirring at RT for 30 min. After that, BTEB (0.3 mL) was added and it was further stirred at RT for 2 h. This mixture was heated statically at 100 °C for 24 h. The obtained Fe_3O_4@SiO_2@CTAB@Ph-PMO product was dispersed in a basic

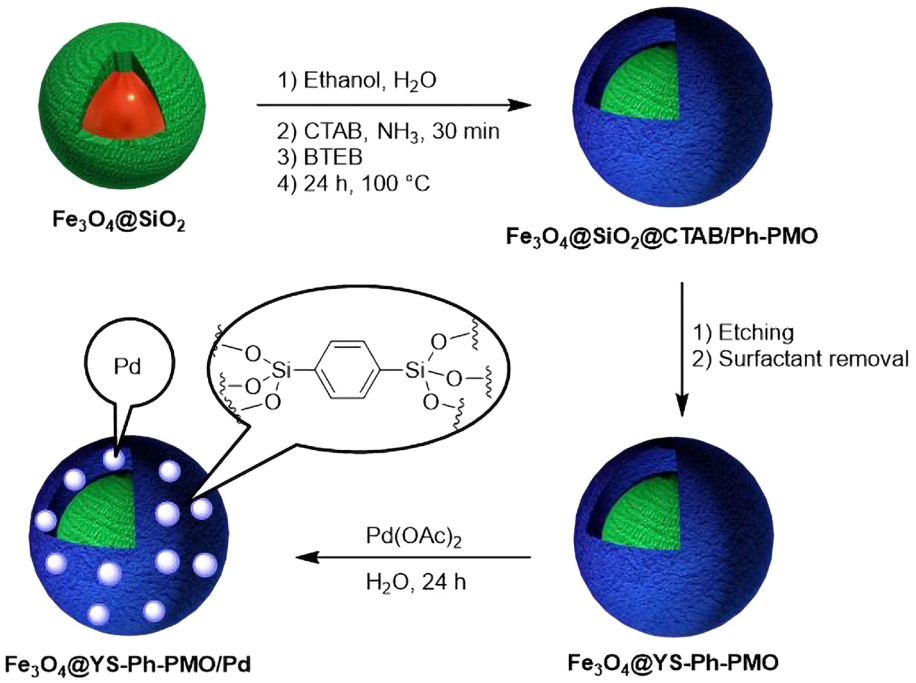

Figure 1. Preparation of Fe_3O_4@YS-Ph-PMO/Pd.

solution (H_2O:Na_2CO_3, 80:4). The resulting mixture was heated to 50 °C for 4 h to eliminate the SiO_2 shell. The CTAB surfactant was successfully eliminated by refluxing of as-made material in an acidic EtOH solution (EtOH:HCl 100:2). The final product was dried at 70 °C for 12 h and denoted as Fe_3O_4@YS-Ph-PMO.

Preparation of Fe_3O_4@YS-Ph-PMO/Pd

For this, Fe_3O_4@YS-Ph-PMO (0.4 g) was added to an aqueous solution of palladium acetate (0.05 M, 14 mL). Then, this mixture was stirred at RT for 24 h. The product was magnetically collected, washed completely with H_2O, dried at 70 °C for 7 h and denoted as Fe_3O_4@YS-Ph-PMO/Pd.

Procedure for the reduction of nitrobenzenes

For this, nitrobenzene (1 mmol), Fe_3O_4@YS-Ph-PMO/Pd (0.9 mol %) and H_2O (10 mL) were added into a reaction vessel. Then, an aqueous solution of $NaBH_4$ (3 mmol) was added while stirring at RT. After completion of reaction, the catalyst was magnetically separated and the amine product was obtained after extraction with EtOAc and evaporation of solvent. The IR and NMR spectra of prepared aminobenzenes are available in the supporting information.

Results and discussion

The preparation of Fe_3O_4@YS-Ph-PMO/Pd nanocatayst with yolk-shell structure is shown in Fig. 1. At first, the magnetic silica (Fe_3O_4@SiO_2) was prepared by chemical modification of Fe_3O_4 nanoparticles with tetramethoxysilane (TMOS). Then, 1,4-bis(triethoxysilyl)benzene (BTEB) was hydrolyzed and co-condensed on the Fe_3O_4@SiO_2 spheres in the presence of CTAB surfactant in a basic ammonia–water–ethanol solution through sol–gel process. Then, the silica layer was removed in an aqueous solution of Na_2CO_3 through an etching process. After that, the CTAB surfactant was removed by a Soxhlet apparatus to give a yolk-shell structured material called Fe_3O_4@YS-Ph-PMO. The resulting material was then treated with a sub-stoichiometric amount of $Pd(OAc)_2$ in water to produce the Fe_3O_4@YS-Ph-PMO/Pd nanocatalyst.

The Fourier transform infrared (FT-IR) spectra of prepared materials are shown in Fig. 2. For all samples, the Fe–O bond is cleared at 582 cm^{-1}. The band about 3552 cm^{-1} is due to the O–H bonds of material surface. For Fe_3O_4@SiO_2, Fe_3O_4@SiO_2@CTAB@YS-Ph-PMO and Fe_3O_4@YS-Ph-PMO/Pd, the peaks at 1122 and 925 cm^{-1} are attributed to Si–O-Si bonds. The bands at 2924 and 2844 cm^{-1} are related to the C–H vibrations of CTAB surfactant (Fig. 2C). Interestingly, for Fe_3O_4@YS-Ph-PMO/Pd, the latter peaks are eliminated (Fig. 2D), indicating the successful removal of CTAB surfactant during extraction process. For Fe_3O_4@SiO_2@CTAB@YS-Ph-PMO and Fe_3O_4@YS-Ph-PMO/Pd, the peaks observed at 3100 and 1620 cm^{-1} are, respectively, correspond to C–H and C=C vibrations of phenyl rings. These confirm the successful formation of Ph-PMO shell on magnetite NPs. Notably, the Fe–O absorption peaks of Fe_3O_4 and Fe_3O_4@SiO_2 exhibited a slight red shift compared to Fe_3O_4@SiO_2@CTAB@Ph-PMO and Fe_3O_4@YS-Ph-PMO/Pd nanomaterials. This shift is in line with the Bouguer-Beer-Lambert (BBL) law, where spectral positions correspond to sample thickness and absorbing entity concentration. The presence of silica, CTAB, and PMO layers on Fe_3O_4 nanoparticles contributes to this red shift, indicating a modified chemical environment surrounding the nanoparticles[54–56]. Moreover, an increase in layer thickness enhances this effect[57–59].

Figure 3 shows the wide-angle powder X-ray diffraction (PXRD) patterns of Fe_3O_4, Fe_3O_4@SiO_2, Fe_3O_4@YS-Ph-PMO and Fe_3O_4@YS-Ph-PMO/Pd nanomaterials. The PXRD patterns of all the materials showed six sharp peaks at 2θ of 30.38, 35.65, 43.34, 53.9, 57.40 and 62.98°, corresponding to the *Miller indices* of 220, 311, 400, 422, 511, and 440, respectively, which is completely matched with that of the Fe_3O_4 standard sample (JCPDS file No. 19-0629)[60]. This finding proves that the crystalline structure of the magnetic iron oxide NPs is preserved during the modification processes. Additionally, a continuous decrease in the intensity of Fe_3O_4 peaks was observed,

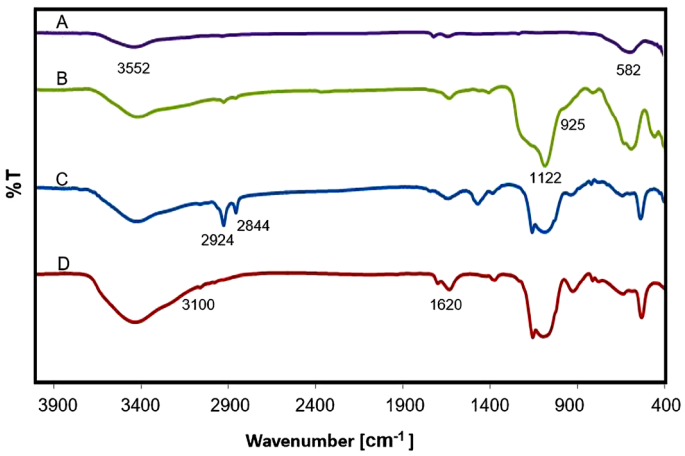

Figure 2. FT-IR spectra of (**A**) Fe_3O_4, (**B**) Fe_3O_4@SiO_2, (**C**) Fe_3O_4@SiO_2@CTAB@Ph-PMO and (**D**) Fe_3O_4@YS-Ph-PMO/Pd.

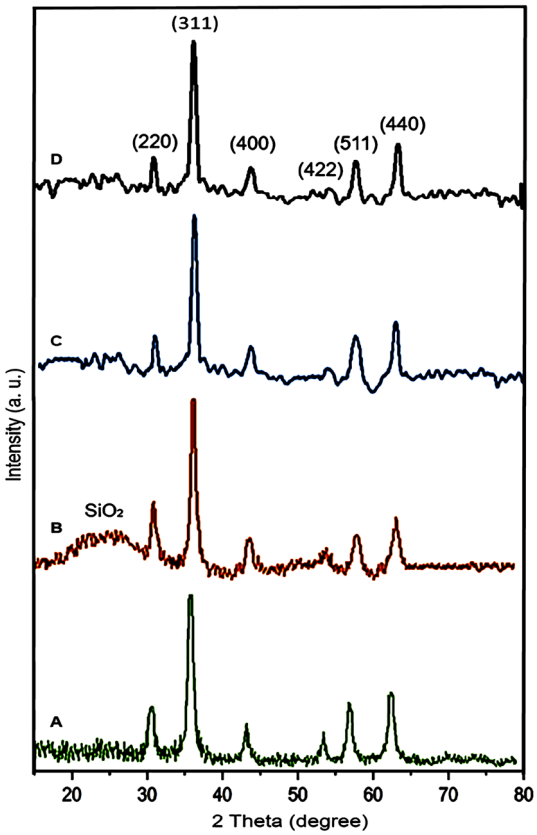

Figure 3. PXRD patterns of (**A**) Fe_3O_4, (**B**) Fe_3O_4@SiO_2, (**C**) Fe_3O_4@YS-Ph-PMO and (**D**) Fe_3O_4@YS-Ph-PMO/Pd.

indicating the successful modification of magnetic iron oxide with the organic and inorganic species. After coating with silica, a new and broad peak at $2\theta = 20–25$ appeared, which is attributed to the presence of amorphous silica (Fig. 3B). This peak disappeared in both Fe_3O_4@YS-Ph-PMO and Fe_3O_4@YS-Ph-PMO/Pd (Fig. 3C and D), confirming the successful removal of the silica layer through the etching process.

The low-angle powder X-ray diffraction (PXRD) pattern of the Fe_3O_4@YS-Ph-PMO/Pd is shown in Fig. 4. This illustrates a broad peak at $2\theta = 2.2°$, which is characteristic of ordered mesoporous structures. This pattern confirm well formation of Ph-PMO shell on magnetite NPs.

Thermal stability of Fe_3O_4@YS-Ph-PMO/Pd was studied by using thermal gravimetric analysis (TGA) (Fig. 5). This showed a low weight loss at temperature below 100 °C, corresponding to removal of adsorbed solvents. The second weight loss observed between 100 to 450 °C is related to the elimination of the remaining CTAB surfactant. The main weight loss, cleared at 451–620 °C, is corresponded to the removal of organic (phenylene)

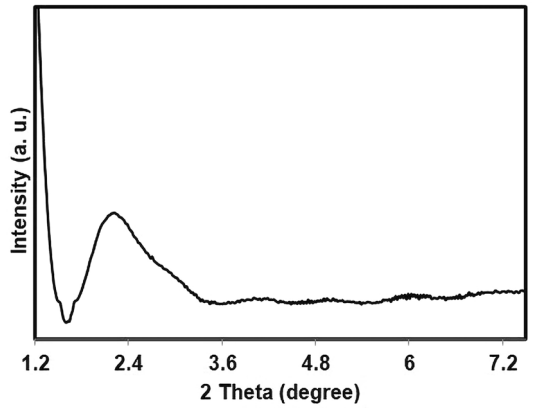

Figure 4. Low-angle PXRD pattern of Fe_3O_4@YS-Ph-PMO/Pd.

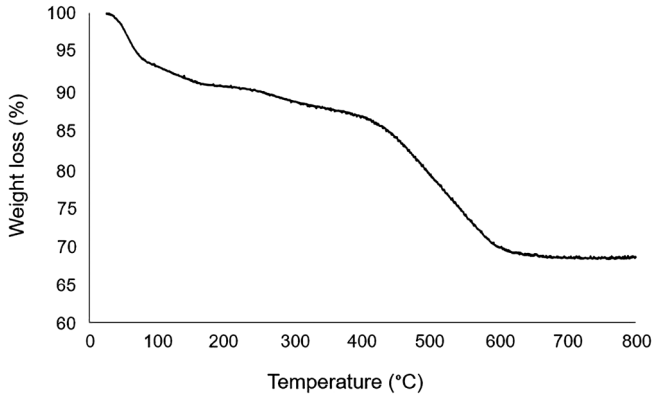

Figure 5. TGA of Fe_3O_4@YS-Ph-PMO/Pd.

moieties incorporated in the mesoporous shell. These data successfully prove the high thermal stability of the designed nanocatalyst.

The magnetic properties of materials were investigated by vibrating sample magnetometer (VSM) (Fig. 6). The saturated magnetization values of the Fe_3O_4 (Fig. 6A), Fe_3O_4@SiO_2 (Fig. 6B) and Fe_3O_4@YS-Ph-PMO/Pd (Fig. 6C) were found to be 65, 30 and 14 emu g^{-1}, respectively. The decrease in magnetic properties following the modification processes is attributed to the well coating of SiO_2 and PMO shells around Fe_3O_4 NPs. The magnetic separation capability of the Fe_3O_4@YS-Ph-PMO/Pd nanocomposite was also evaluated by introducing an external magnet near the reaction vessel, as depicted in Fig. 6b. As demonstrated, these nanomaterials can be efficiently collected by using an external magnet within seconds, confirming the high magnetic properties of the designed catalyst, rendering it readily recoverable.

The scanning electron microscopy (SEM) was performed to study the morphology of the particles at different steps of nanocatalyst preparation. According to this analysis, a uniform spherical morphology was observed for all prepared nanomaterials with an increase in size observed at each step (Fig. 7). The progressive increase in particle size after each step confirms the successful formation of the shell and modification of magnetite nanoparticles, as outlined in Fig. 1.

The TEM image of the Fe_3O_4@YS-Ph-PMO/Pd nanocatalyst showed spherical particles with a black core (magnetite NPs) and a grey shell (PMO layer) for the designed nanocomposite (Fig. 8). Notably, recently, the similar TEM images have been reported for a number of yolk-shell structured magnetic nanocomposites[61,62].

The Fe_3O_4@YS-Ph-PMO/Pd nanocatalyst was then employed in the reduction of nitroarenes in the presence of $NaBH_4$ (Table 1). The effect of different parameters was studied in the reduction of nitrobenzene as a reaction model. As shown, in the absence of catalyst, along with 3 mmol of $NaBH_4$, no reduction was observed (Table 1, entry 1). However, after addition of the catalyst, the reaction proceeded successfully, and the highest yield

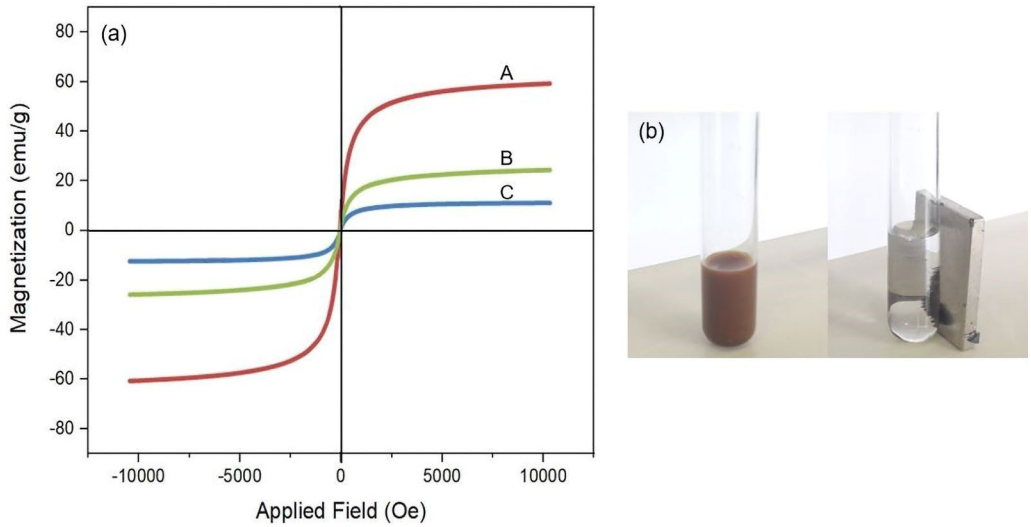

Figure 6. (**a**) VSM diagrams of Fe_3O_4 (A), Fe_3O_4@SiO_2 (B) and Fe_3O_4@YS-Ph-PMO/Pd (C) nanomaterials and (**b**) magnetic separation ability of Fe_3O_4@YS-Ph-PMO/Pd nanocatalyst.

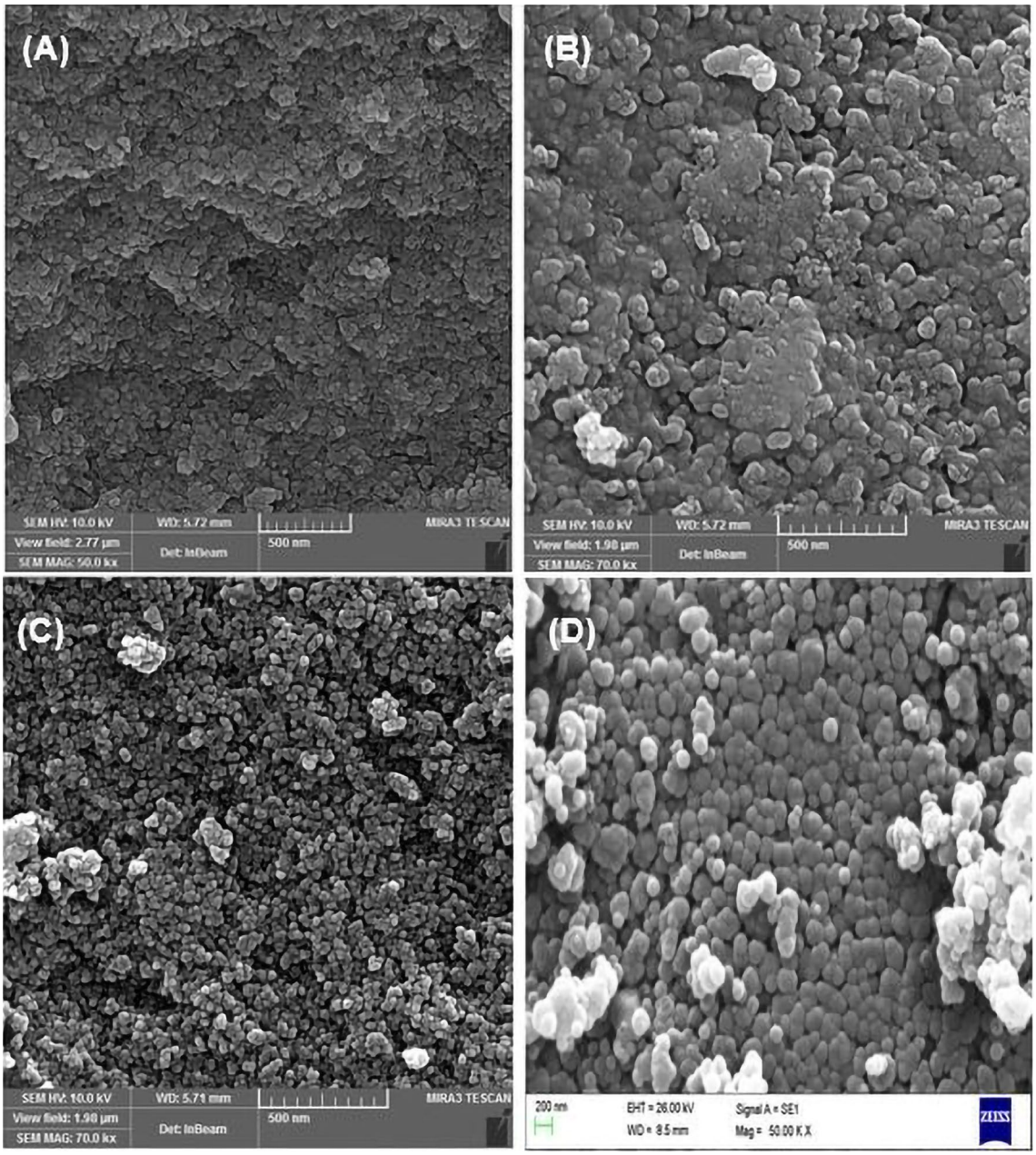

Figure 7. SEM images of (**A**) Fe_3O_4, (**B**) Fe_3O_4@SiO_2, (**C**) Fe_3O_4@YS-Ph-PMO and (**D**) Fe_3O_4@YS-Ph-PMO/Pd.

achieved using 0.9 mol% of the Fe_3O_4@YS-Ph-PMO/Pd (Table 1, entry 3). Next, the effect of different solvents including methanol, ethanol and water was tested. As depicted in Table 1, the use of MeOH, EtOH, aqueous methanol or ethanol, as well as solvent-free media, resulted in low to moderate yields (Table 1, entries 5–9). Pleasantly, in aqueous media at RT, the reaction was completed and excellent yield of aniline was obtained. To investigate the neat effect of Pd, the efficiency of Fe_3O_4@YS-Ph-PMO/Pd was compared with Fe_3O_4 and Fe_3O_4@YS-Ph-PMO nanomaterials. This demonstrated that when using Pd-free Fe_3O_4 and Fe_3O_4@Ph-PMO materials, the reaction did not progress, and only a trace conversion (< 4%) was observed (Table 1, entries 10 and 11). This confirms that the reduction process is catalyzed by supported palladium species. Based on the aforementioned results, $NaBH_4$ (3 mmol), H_2O solvent (3 mL), Fe_3O_4@YS-Ph-PMO/Pd catalyst (0.9 mol %) and RT were chosen as the optimum conditions (Table 1, entry 3).

The efficiency and the scope of the Fe_3O_4@YS-Ph-PMO/Pd nanocatalyst were next studied using a variety of nitrobenzenes (Table 2). As shown, all nitroarenes deliver corresponding anilines in high yields. Importantly, in all cases, it was found that the aniline derivatives were the only products of the reactions. These results demonstrate high selectivity of the designed catalytic system.

Recoverability and reusability of the Fe_3O_4@YS-Ph-PMO/Pd nanocatalyst in the reduction of nitrobenzene were also examined. For this, after completion of the reaction, the Fe_3O_4@YS-Ph-PMO/Pd catalyst was

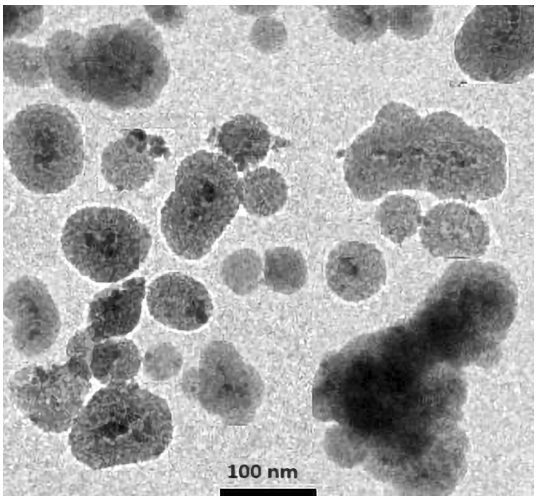

Figure 8. TEM image of the Fe_3O_4@YS-Ph-PMO/Pd nanocatalyst.

Entry	Catalyst	Catalyst loading (mol %)	Time (min)	Solvent	Temperature	Yield (%.)[b]
1	–	–	300	H_2O	Reflux	N. R.
2	Fe_3O_4@YS-Ph-PMO/Pd	0.6	10	H_2O	RT	78
3	Fe_3O_4@YS-Ph-PMO/Pd	0.9	10	H_2O	RT	96
4	Fe_3O_4@YS-Ph-PMO/Pd	1.2	10	H_2O	RT	96
5	Fe_3O_4@YS-Ph-PMO/Pd	0.9	10	Solvent-free	RT	63
6	Fe_3O_4@YS-Ph-PMO/Pd	0.9	10	MeOH	RT	57
7	Fe_3O_4@YS-Ph-PMO/Pd	0.9	10	MeOH/H_2O	RT	75
8	Fe_3O_4@YS-Ph-PMO/Pd	0.9	10	EtOH	RT	68
9	Fe_3O_4@YS-Ph-PMO/Pd	0.9	10	EtOH/H_2O	RT	92
10	Fe_3O_4	0.03 g	10	H_2O	RT	Trace
11	Fe_3O_4@YS-Ph-PMO	0.03 g	10	H_2O	RT	Trace

Table 1. Reduction of nitrobenzene in the presence of Fe_3O_4@YS-Ph-PMO/Pd[a]. [a]Nitrobenzene (1 mmol), $NaBH_4$ (3 mmol), Fe_3O_4@YS-Ph-PMO/Pd nanocatalyst and solvent (3 mL). [b]Isolated yields.

magnetically separated, washed and reused in the next run. It was found that the Fe_3O_4@YS-Ph-PMO/Pd catalyst can be recovered and reused for at least 11 times with no important decrease in efficiency (Fig. 9).

A leaching experiment was then accomplished on the model reaction to investigate the leaching behavior of the palladium species under applied conditions. For this, after a conversion of about 40%, the Fe_3O_4@YS-Ph-PMO/Pd catalyst was magnetically separated and the residue mixture was allowed to progress under the optimized conditions. Notably, after 140 min, no further product was observed indicating that the removal of the catalyst resulted in a complete stop of the conversion of nitrobenzene to aniline (Fig. 10). These results confirm no leaching of palladium species and also demonstrate the high stability of the designed catalyst under applied conditions.

The catalytic performance of Fe_3O_4@YS-Ph-PMO/Pd was also compared with former heterogeneous catalysts in the reduction of nitrobenzene (Table 3). The result showed that the efficiency of Fe_3O_4@YS-Ph-PMO/Pd is much better than previous catalytic systems, particularly in terms of reaction temperature and recovery times.

Conclusion

In this work, the preparation, characterization and application of a new nanocatalyst named Fe_3O_4@YS-Ph-PMO/Pd were developed. The FT-IR and TG analyses clearly demonstrated high stability and well incorporation/immobilization of expected organic and inorganic moieties onto/into prepared nanomaterial. The SEM and TEM images showed a spherical morphology for the designed catalyst. The VSM analysis confirmed well-magnetic properties of the catalyst. The wide-angle PXRD analysis confirmed high stability of crystalline structure of magnetite NPs during catalyst preparation steps. The Fe_3O_4@YS-Ph-PMO/Pd was powerfully used in the reduction of nitrobenzenes giving corresponding anilines in high yield and selectivity. The leaching and recovery experiments confirmed that the designed catalyst operate in a heterogeneous manner. Other advantages of this methodology were the use of water as green solvent, performing reactions at RT, short reaction times, clean conditions, as well as high recoverability, durability and stability of the designed catalyst. Some applications of this catalytic system in other organic processes are underway in our laboratory.

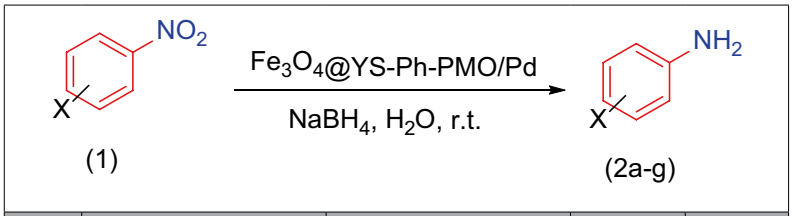

Entry	Substrate	Product	Time (min)	Yield (%)[b]
1	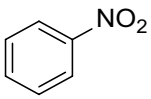	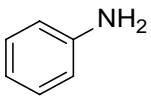	10	96
2	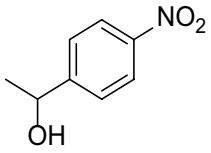	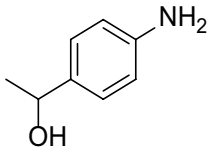	12	96
3	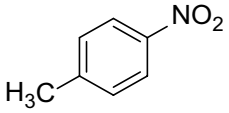	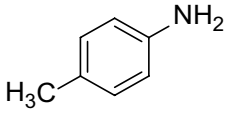	12	94
4	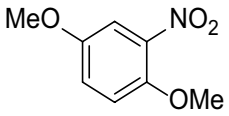	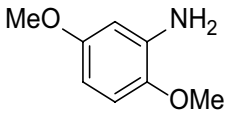	15	93
5	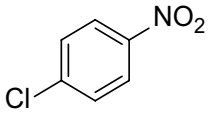	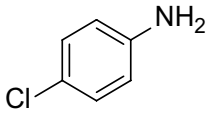	14	95
6	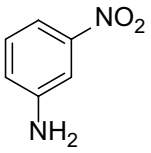	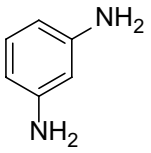	15	91
7	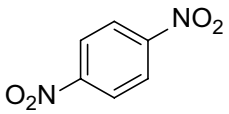	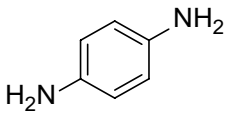	18	92

Table 2. Reduction of different nitrobenzenes using Fe_3O_4@YS-Ph-PMO/Pd catalyst[a]. [a]Nitrobenzene (1 mmol), $NaBH_4$ (3 mmol), H_2O (3 mL) and catalyst (0.9 mol%). [b]Isolated yields.

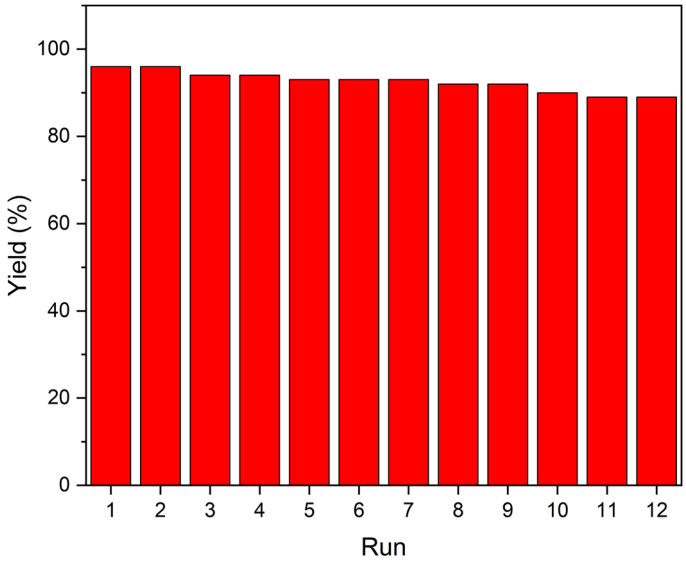

Figure 9. Recoverability and reusability of the Fe_3O_4@YS-Ph-PMO/Pd nanocatalyst in the reduction of nitrobenzene.

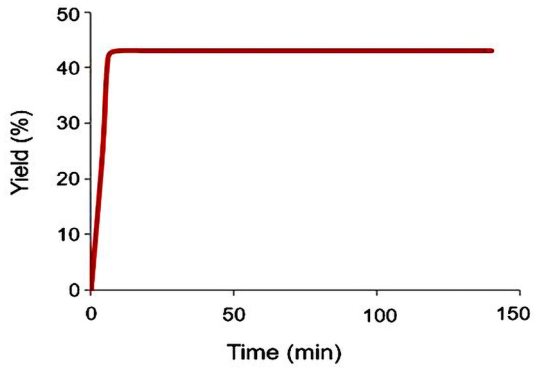

Figure 10. Result of the leaching test in the reduction of nitrobenzene in the presence of Fe_3O_4@YS-Ph-PMO/Pd nanocatalyst.

Entry	Catalyst	Conditions	Recovery times	Refs.
1[a]	γ-Fe_2O_3@SiO_2–Pt@$mSiO_2$	Hydrogen gas, EtOH, 40 °C	5	63
2[b]	γ-Fe_2O_3-MNAs	$MeNHNH_2$, EtOH, 60 °C	7	64
3[c]	$RHPrNH_2$@Ag	$NaBH_4$, H_2O, Reflux	4	65
4[d]	Fe_3O_4@nSiO_2@mSiO_2/Pr-Imi-NH_2·Ag	$NaBH_4$, H_2O, 95 °C	4	66
5	Pd/SBA-15	Hydrogen gas, decane, EtOH, 313 K	5	67
6	Pt–Pd/PMO-SBA-15	Hydrogen gas, EtOH, 60 °C	5	68
7	Fe_3O_4@YS-Ph-PMO/Pd	$NaBH_4$, H_2O, RT	11	This work

Table 3. Comparison of catalytic activity of Fe_3O_4@YS-Ph-PMO/Pd nanocatalyst with previously reported catalytic systems in the reduction of nitrobenzene. [a]$mSiO_2$, mesoporous silica. [b]MNAs, mesoporous nanoparticle assemblies. [c]$RHPrNH_2$, rice husk-SiO_2 aminopropylsilane. [d]Pr-Imi, propylimidazolium.

Data availability

All data and materials are included in the manuscript.

Received: 30 January 2024; Accepted: 4 July 2024
Published online: 15 July 2024

References

1. Zhao, Y. & Jiang, L. Hollow micro/nanomaterials with multilevel interior structures. *Adv. Mater.* **21**, 3621–3638 (2009).
2. Lou, X. W. D., Archer, L. A. & Yang, Z. Hollow micro-/nanostructures: Synthesis and applications. *Adv. Mater.* **20**, 3987–4019 (2008).
3. Liu, J., Qiao, S. Z., Hu, Q. H. & Lu, G. Q. Magnetic nanocomposites with mesoporous structures: Synthesis and applications. *Small* **7**, 425–443 (2011).
4. An, K. & Hyeon, T. Synthesis and biomedical applications of hollow nanostructures. *Nano Today* **4**, 359–373 (2009).
5. Liu, J. *et al.* Yolk/shell nanoparticles: New platforms for nanoreactors, drug delivery and lithium-ion batteries. *Chem. Commun.* **47**, 12578–12591 (2011).
6. Zou, H. *et al.* An organosilane-directed growth-induced etching strategy for preparing hollow/yolk–shell mesoporous organosilica nanospheres with perpendicular mesochannels and amphiphilic frameworks. *J. Mater. Chem. A* **2**, 12403–12412 (2014).
7. Mirbagheri, R., Elhamifar, D. & Shaker, M. Yolk–shell structured magnetic mesoporous silica: A novel and highly efficient adsorbent for removal of methylene blue. *Sci. Rep.* **11**, 23259. https://doi.org/10.1038/s41598-021-02699-w (2021).
8. Neysi, M. & Elhamifar, D. Yolk-shell structured magnetic mesoporous organosilica supported ionic liquid/Cu complex: An efficient nanocatalyst for the green synthesis of pyranopyrazoles. *Front. Chem.* **11**, 125 (2023).
9. Peng, H. *et al.* Multifunctional yolk-shell structured magnetic mesoporous polydopamine/carbon microspheres for photothermal therapy and heterogenous catalysis. *ACS Appl. Mater. Interfaces* **14**, 23888–23895 (2022).
10. Liu, J., Bai, S., Zhong, H., Li, C. & Yang, Q. Tunable assembly of organosilica hollow nanospheres. *J. Phys. Chem. C* **114**, 953–961 (2009).
11. Liu, J. *et al.* Organic–inorganic hybrid hollow nanospheres with microwindows on the shell. *Chem. Mater.* **20**, 4268–4275 (2008).
12. Wei, Y. *et al.* A versatile in situ etching-growth strategy for synthesis of yolk–shell structured periodic mesoporous organosilica nanocomposites. *RSC Adv.* **6**, 51470–51479 (2016).
13. Song, J.-C., Xue, F.-F., Zhang, X.-X., Lu, Z.-Y. & Sun, Z.-Y. Synthesis of yolk–shell mesoporous silica nanoparticles via a facile one-pot approach. *Chem. Commun.* **53**, 3761–3764 (2017).
14. Liu, B. & Zeng, H. C. Symmetric and asymmetric Ostwald ripening in the fabrication of homogeneous core–shell semiconductors. *Small* **1**, 566–571 (2005).
15. Ding, S. *et al.* Formation of SnO2 hollow nanospheres inside mesoporous silica nanoreactors. *J. Am. Chem. Soc.* **133**, 21–23 (2010).
16. Yin, Y. *et al.* Formation of hollow nanocrystals through the nanoscale Kirkendall effect. *Science* **304**, 711–714 (2004).
17. Chen, D., Li, L., Tang, F. & Qi, S. Facile and scalable synthesis of tailored silica "nanorattle" structures. *Adv. Mater.* **21**, 3804–3807 (2009).
18. Zhu, Y., Kockrick, E., Ikoma, T., Hanagata, N. & Kaskel, S. An efficient route to rattle-type Fe3O4@ SiO2 hollow mesoporous spheres using colloidal carbon spheres templates. *Chem. Mater.* **21**, 2547–2553 (2009).
19. Yang, Y., Liu, J., Li, X., Liu, X. & Yang, Q. Organosilane-assisted transformation from core–shell to yolk–shell nanocomposites. *Chem. Mater.* **23**, 3676–3684 (2011).
20. Wang, X., Feng, J., Bai, Y., Zhang, Q. & Yin, Y. Synthesis, properties, and applications of hollow micro-/nanostructures. *Chem. Rev.* **116**, 10983–11060 (2016).
21. Purbia, R. & Paria, S. Yolk/shell nanoparticles: Classifications, synthesis, properties, and applications. *Nanoscale* **7**, 19789–19873 (2015).
22. Yang, L., Guo, H., Wang, L. & Zhang, J. A facile "polystyrene-dissolving" strategy to hollow periodic mesoporous organosilica with flexible structure-tailorability. *Micropor. Mesopor. Mat* **239**, 173–179 (2017).
23. Dai, J. *et al.* Yolk–shell Fe 3 O 4@ SiO 2@ PMO: Amphiphilic magnetic nanocomposites as an adsorbent and a catalyst with high efficiency and recyclability. *Green Chem.* **19**, 1336–1344 (2017).
24. Wang, H. *et al.* Preparation of highly dispersed W/Al2O3 hydrodesulfurization catalysts via a microwave hydrothermal method: Effect of oxalic acid. *Arab. J. Chem.* **9**, 18–24. https://doi.org/10.1016/j.arabjc.2014.11.023 (2016).
25. Liu, J., Qiao, S. Z., Budi-Hartono, S. & Lu, G. Q. M. Monodisperse yolk–shell nanoparticles with a hierarchical porous structure for delivery vehicles and nanoreactors. *Angew. Chem.* **122**, 5101–5105 (2010).
26. Pandarus, V., Ciriminna, R., Beland, F. & Pagliaro, M. A new class of heterogeneous platinum catalysts for the chemoselective hydrogenation of nitroarenes. *Adv. Synth. Catal.* **353**, 1306–1316 (2011).
27. Mikami, Y. *et al.* Highly chemoselective reduction of nitroaromatic compounds using a hydrotalcite-supported silver-nanoparticle catalyst under a CO atmosphere. *Chem. Lett.* **39**, 223–225 (2010).
28. Ono, N. *The Nitro-Aldol (Henry) Reaction. The Nitro Group in Organic Synthesis* 30 (Wiley-VCH, 2001).
29. Lawrence, S. A. *Amines: Synthesis, Properties and Applications* (Cambridge University Press, 2004).
30. Mohan, V. *et al.* Advantage of Ni/SBA-15 catalyst over Ni/MgO catalyst in terms of catalyst stability due to release of water during nitrobenzene hydrogenation to aniline. *Catal. Commun.* **18**, 89–92 (2012).
31. Zengin, N., Göksu, H. & Şen, F. Chemoselective hydrogenation of aromatic nitro compounds in the presence of homogeneous Pd based catalysts. *Chemosphere* **282**, 130887 (2021).
32. Loghmani, M. H. & Shojaei, A. F. Hydrogen production through hydrolysis of sodium borohydride: Oleic acid stabilized Co–La–Zr–B nanoparticle as a novel catalyst. *Energy* **68**, 152–159 (2014).
33. Shil, A. K., Sharma, D., Guha, N. R. & Das, P. Solid supported Pd (0): An efficient recyclable heterogeneous catalyst for chemoselective reduction of nitroarenes. *Etrahedron. Lett.* **53**, 4858–4861 (2012).
34. Fountoulaki, S. *et al.* Mechanistic studies of the reduction of nitroarenes by NaBH4 or hydrosilanes catalyzed by supported gold nanoparticles. *ACS Catal.* **4**, 3504–3511 (2014).
35. Schlesinger, H. *et al.* Sodium borohydride, its hydrolysis and its use as a reducing agent and in the generation of hydrogen1. *J. Am. Chem. Soc.* **75**, 215–219 (1953).
36. Saavedra, J. Z. *et al.* Reaction of InCl3 with various reducing agents: InCl3–NaBH4-mediated reduction of aromatic and aliphatic nitriles to primary amines. *J. Org. Chem.* **77**, 221–228 (2011).
37. Wang, P., Liu, H., Niu, J., Li, R. & Ma, J. Entangled Pd complexes over Fe 3 O 4@ SiO 2 as supported catalysts for hydrogenation and Suzuki reactions. *Catal. Sci. Tech.* **4**, 1333–1339 (2014).
38. Lin, F.-H. & Doong, R.-A. Catalytic nanoreactors of Au@ Fe3O4 yolk-shell nanostructures with various au sizes for efficient nitroarene reduction. *J. Phys. Chem. C* **121**, 7844–7853 (2017).
39. Lopes, R., Pereira, M. M. & Royo, B. Selective reduction of nitroarenes with silanes catalyzed by nickel N-heterocyclic carbene complexes. *ChemCatChem* **9**, 3073–3077 (2017).
40. Kadam, H. K. & Tilve, S. G. Advancement in methodologies for reduction of nitroarenes. *RSC Adv.* **5**, 83391–83407 (2015).

41. Gawande, M. B. *et al.* Regio-and chemoselective reduction of nitroarenes and carbonyl compounds over recyclable magnetic ferrite nickel nanoparticles (Fe3O4 Ni) by using glycerol as a hydrogen source. *Chem.-A Eur. J.* **18**, 12628–12632 (2012).
42. Jang, Y. *et al.* Simple one-pot synthesis of Rh–Fe 3 O 4 heterodimer nanocrystals and their applications to a magnetically recyclable catalyst for efficient and selective reduction of nitroarenes and alkenes. *Chem. Commun.* **47**, 3601–3603 (2011).
43. Zhang, H., Gao, S., Shang, N., Wang, C. & Wang, Z. Copper ferrite–graphene hybrid: A highly efficient magnetic catalyst for chemoselective reduction of nitroarenes. *RSC Adv.* **4**, 31328–31332 (2014).
44. Feng, C., Zhang, H.-Y., Shang, N.-Z., Gao, S.-T. & Wang, C. Magnetic graphene nanocomposite as an efficient catalyst for hydrogenation of nitroarenes. *Chin. Chem. Lett.* **24**, 539–541 (2013).
45. Choi, Y. *et al.* Hybrid gold nanoparticle-reduced graphene oxide nanosheets as active catalysts for highly efficient reduction of nitroarenes. *J. Mater. Chem.* **21**, 15431–15436 (2011).
46. He, G. *et al.* Fe 3 O 4@ graphene oxide composite: A magnetically separable and efficient catalyst for the reduction of nitroarenes. *Mater. Res. Bull.* **48**, 1885–1890 (2013).
47. Gawande, M. B. *et al.* First application of core-shell Ag@ Ni magnetic nanocatalyst for transfer hydrogenation reactions of aromatic nitro and carbonyl compounds. *RSC Adv.* **3**, 1050–1054 (2013).
48. Zeynizadeh, B., Mohammadzadeh, I., Shokri, Z. & Hosseini, S. A. Synthesis and characterization of NiFe 2 O 4@ Cu nanoparticles as a magnetically recoverable catalyst for reduction of nitroarenes to arylamines with NaBH 4. *J. Colloid Interface Sci.* **500**, 285–293 (2017).
49. Mirbagheri, R., Elhamifar, D. & Hajati, S. Ru-containing magnetic yolk–shell structured nanocomposite: A powerful, recoverable and highly durable nanocatalyst. *RSC Adv.* **11**, 10243–10252 (2021).
50. Norouzi, M. & Elhamifar, D. Magnetic yolk-shell structured methylene and propylamine based mesoporous organosilica nanocomposite: A highly recoverable and durable nanocatalyst with improved efficiency. *Colloids Surfaces A: Physicochem. Eng. Aspects* **615**, 126226 (2021).
51. Haydari, Z., Elhamifar, D., Shaker, M. & Norouzi, M. Magnetic nanoporous MCM-41 supported melamine: A powerful nanocatalyst for synthesis of biologically active 2-amino-3-cyanopyridines. *Appl. Surface Sci. Adv.* **5**, 100096 (2021).
52. Elhamifar, D., Ramazani, Z., Norouzi, M. & Mirbagheri, R. Magnetic iron oxide/phenylsulfonic acid: A novel, efficient and recoverable nanocatalyst for green synthesis of tetrahydrobenzo[b]pyrans under ultrasonic conditions. *J. Colloid Interface Sci.* **511**, 392–401. https://doi.org/10.1016/j.jcis.2017.10.013 (2018).
53. Norouzi, M., Elhamifar, D., Mirbagheri, R. & Ramazani, Z. Synthesis, characterization and catalytic application of a novel ethyl and boron sulfonic acid based bifunctional periodic mesoporous organosilica. *J. Taiwan Inst. Chem. Eng.* **89**, 234–244. https://doi.org/10.1016/j.jtice.2018.05.011 (2018).
54. Asadbegi, S., Bodaghifard, M. A. & Mobinikhaledi, A. Poly N, N-dimethylaniline-formaldehyde supported on silica-coated magnetic nanoparticles: A novel and retrievable catalyst for green synthesis of 2-amino-3-cyanopyridines. *Res. Chem. Intermed.* **46**, 1629–1643. https://doi.org/10.1007/s11164-017-3200-4 (2020).
55. Akhavan, M., Foroughifar, N., Pasdar, H., Khajeh-Amiri, A. & Bekhradnia, A. Copper(II)-complex functionalized magnetite nanoparticles: A highly efficient heterogeneous nanocatalyst for the synthesis of 5-arylidenthiazolidine-2,4-diones and 5-arylidene-2-thioxothiazolidin-4-one. *Trans. Metal Chem.* **42**, 543–552. https://doi.org/10.1007/s11243-017-0159-3 (2017).
56. Neysi, M., Zarnegaryan, A. & Elhamifar, D. Core–shell structured magnetic silica supported propylamine/molybdate complexes: An efficient and magnetically recoverable nanocatalyst. *New J. Chem.* **43**, 12283–12291. https://doi.org/10.1039/C9NJ01160A (2019).
57. Mayerhöfer, T. G., Pahlow, S., Hübner, U. & Popp, J. R. CaF2: An ideal substrate material for infrared spectroscopy?. *Anal. Chem.* **92**, 9024–9031 (2020).
58. Mayerhöfer, T. G. & Popp, J. The electric field standing wave effect in infrared transflection spectroscopy. *Spectrochim. Acta A Mol. Biomol. Spectrosc.* **191**, 283–289 (2018).
59. Mayerhöfer, T. G., Pahlow, S., Hübner, U. & Popp, J. Removing interference-based effects from the infrared transflectance spectra of thin films on metallic substrates: A fast and wave optics conform solution. *Analyst* **143**, 3164–3175 (2018).
60. Kassaee, M., Masrouri, H. & Movahedi, F. Sulfamic acid-functionalized magnetic Fe3O4 nanoparticles as an efficient and reusable catalyst for one-pot synthesis of α-amino nitriles in water. *Appl. Catal. A* **395**, 28–33 (2011).
61. Yue, Q. *et al.* Plasmolysis-inspired nanoengineering of functional yolk–shell microspheres with magnetic core and mesoporous silica shell. *J. Am. Chem. Soc.* **139**, 15486–15493 (2017).
62. Yu, L. *et al.* Nonsacrificial self-template synthesis of colloidal magnetic yolk–shell mesoporous organosilicas for efficient oil/water interface catalysis. *Small* **15**, 1805465 (2019).
63. Jin, C. *et al.* Versatile rattle-type magnetic mesoporous silica spheres, working as adsorbents and nanocatalyst containers. *J. Sol-Gel Sci. Technol.* **77**, 279–287 (2016).
64. Papadas, I. T., Fountoulaki, S., Lykakis, I. N. & Armatas, G. S. Controllable synthesis of mesoporous iron oxide nanoparticle assemblies for chemoselective catalytic reduction of nitroarenes. *Chem. Eur. J.* **22**, 4600–4607 (2016).
65. Davarpanah, J. & Kiasat, A. R. Catalytic application of silver nanoparticles immobilized to rice husk-SiO 2-aminopropylsilane composite as recyclable catalyst in the aqueous reduction of nitroarenes. *Catal. Commun.* **41**, 6–11 (2013).
66. Nasab, M. J. & Kiasat, A. R. Multifunctional Fe 3 O 4@ n SiO 2@ m SiO 2/Pr-Imi-NH 2· Ag core–shell microspheres as highly efficient catalysts in the aqueous reduction of nitroarenes: Improved catalytic activity and facile catalyst recovery. *RSC Adv.* **6**, 41871–41877 (2016).
67. Duan, Y. *et al.* Synthesis of Pd/SBA-15 catalyst employing surface-bonded vinyl as a reductant and its application in the hydrogenation of nitroarenes. *RSC Adv.* **7**, 3443–3449 (2017).
68. Liu, C., Tan, R., Yu, N. & Yin, D. Pt–Pd bi-metal nanoparticles captured and stabilized by imine groups in a periodic mesoporous organosilica of SBA-15 for hydrogenation of nitrobenzene. *Micropor. Mesopor. Mater.* **131**, 162–169 (2010).

Acknowledgements

The authors thank Yasouj University and Iran National Science Foundation (INSF) for supporting this work.

Author contributions

M. N.: Writing Original Draft, Investigation, Resources, Formal analysis. D. E.: Conceptualization, Writing, Review & Editing, Supervision, Visualization. S. K.: Formal Analysis, Revising Original Draft.

Competing interests

The authors declare no competing interests.

Additional information

Supplementary Information The online version contains supplementary material available at https://doi.org/10.1038/s41598-024-66883-4.

Correspondence and requests for materials should be addressed to D.E.